



An advanced Backstepping Control Scheme via Active and Reactive Powers for DFIM-Based on Variable-Speed Turbine Energy

Sara Kadi^a, Habib Benbouhenn^b, I. Hamdan^{c, d}, Emad Abdelkarim^{c, e*}

^aPower equipments Characterization and Diagnosis Laboratory (USTHB), Algiers, Algeria

^bElectrical & Electronics Engineering, Nisantasi University, Istanbul, Turkey

^cDepartment of Electrical Engineering, College of Engineering and Information Technology, Buraydah Private Colleges, Buraydah 51418, kingdom of Saudi Arabia

^dDepartment of Electrical Engineering, Faculty of Engineering, South Valley University, Qena 83523, Egypt

^eDepartment of Electrical Engineering, Faculty of Engineering, Aswan university, Aswan, Egypt

Abstract

This paper presents a control scheme using active and reactive power control with advanced backstepping control of doubly-fed induction machine (DFIM) based on variable-speed wind-energy-conversion system (WECS). The modelling and control of WECS are introduced using DFIM with back-to-back converters for a variable-speed application. Also, the aim is to design and compare two-distinct decoupling control strategy to control the rotor-side converter with integral proportional (PI) control (indirect control) strategy and nonlinear integral backstepping control strategy, this system employs a maximum power-point tracking (MPPT) strategy to maximize the extraction of power during the conversion process. The proposed studied system is tested using MATLAB/Simulink in terms of decoupling, the robustness against-parameters variations and the reference-tracking stability. This results is completed by a comparative study which reflect the better performance of studied control method. According to simulation data, the control scheme improves DFIM-turbine system performance.

© 2025 Published by Published by Faculty of Engineering – Sohag University. DOI: 10.21608/sej.2024.338390.1071

Keywords: Wind Energy System; Doubly-Fed Induction Generator; PI control; MPPT; Integral Backstepping Control.

5. INTRODUCTION

Renewable energies refer to a group of methods for generating energy from resources or sources that are, in theory, limitless, available at all times, or reusable more quickly than they are used up [1]. Renewable energy is generated from potentially limitless sources on a human scale, such as the sun's beams or the wind's speeds. Double-fed induction machines (DFIM) are a common feature of wind turbines that are currently in use [2].

Variable-speed turbines commonly use DFIM because they can operate effectively across a wide range of speeds. Additionally, the rotor converters are designed to handle only 20% to 30% of the total power that is nominal. This design significantly decreases both energy losses and overall system costs, making it a more efficient choice [1,2].

To maximize wind energy extraction and maintain a unity power factor, the DFIM employs Stator Voltage-Orientation (SVO) or Stator Flux-Orientation (SFO) techniques, optimizing control strategies for enhanced performance and efficiency [1, 3], which allowed to control independently the active and reactive power [4, 5]. This transformation is combined with integral proportional (PI)-controller which assembles inner-loop for rotor currents control and outer-loop for reactive and active powers control.

Variable-speed turbines commonly use DFIG because they can operate effectively across a wide range of speeds. Using the Maximum Power Point Tracking (MPPT) technique, it effectively keeps the power coefficient at its optimal level [6-10].

The conventional PI-controller has good performers, low costs and it is easy to maintain, therefore it's the most used for industrial applications [6-14]. However, the performance is highly reliant on machine parameters, and any variations in these parameters can lead to deterioration in functionality, affecting the overall effectiveness

* Corresponding author: emad.hussein2011@gmail.com.

and efficiency of the system. Accurate parameter management is crucial for optimal operation [15-20]. Numerous control strategies have been put forth for DFIM with wind turbine systems [18-25].

To tackle this challenge, a nonlinear Backstepping controller incorporating integral actions associated with a Lyapunov function has been suggested to maintain the stability of the entire system. This method ensures that the system remains globally stable, even when faced with variations in parameters. By utilizing this approach, stability can be achieved within a finite period, effectively enhancing the system's resilience against changes and uncertainties in its parameters [1,14].

This paper presents a description and modelling of the wind turbine linked to DFIM in the d-q Park reference frame. The PI controller (indirect-control) than the integral backstepping controller are tested and compared for active and reactive power independently control by using a stator flux-oriented strategy applied to the rotor side converter. The dynamic performance is analyzed by MATLAB-Simulink software. The outcome is supplemented by a comparative analysis that demonstrates the effectiveness of the advanced backstepping control scheme.

The remaining part of this paper is organized as follows. In Section 2, the description and modelling of variable-speed turbine energy is introduced. The vector control of DFIM, PI-control strategy and advanced nonlinear-integral backstepping of DFIM are studied, respectively in Section 3. The results obtained are discussed and presented in Section 4. Conclusion is described in Section 5.

2. DESCRIPTION AND MODELLING OF THE VARIABLE-SPEED TURBINE ENERGY

The system is shown in (Fig.1); the DFIM is connected to grid by its rotor which is connected to two-converters (back-to-back), while the stator circuit is directly connected to the power grid.

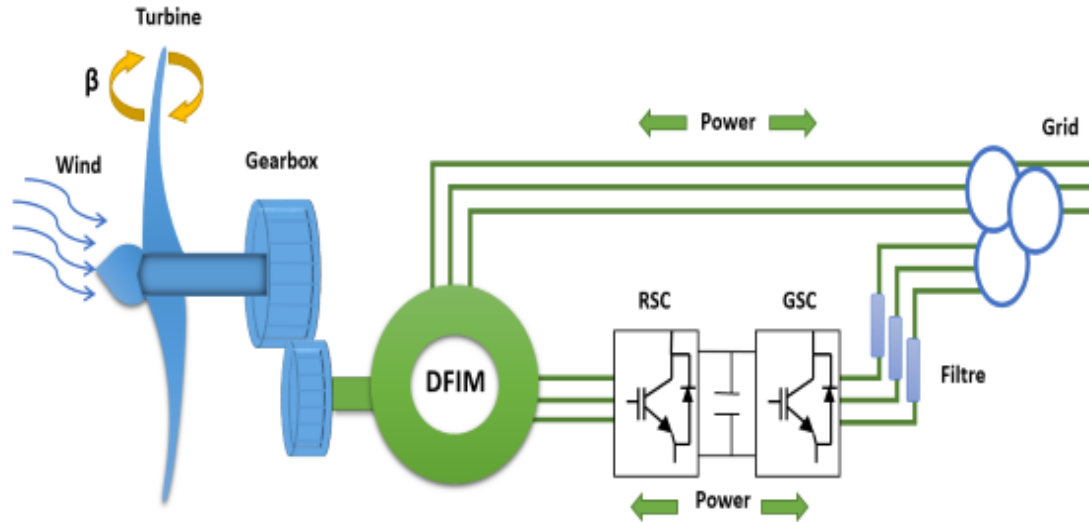


Fig. 1. Wind Energy System.

The wind-turbine mathematical model is defined as follow [8-10]:

$$P_V = \frac{\rho S V^3}{2} \quad (1)$$

$$P_{aer} = C_p P_V = \frac{1}{2} \rho \pi R^2 V^3 C_p(\lambda, \beta) \quad (2)$$

The aerodynamic power-coefficient C_p depends on the Tip Speed Ratio λ (TSR) and the blade-pitch angle (β) is giving by [2,14]:

$$C_p(\lambda, \beta) = (0.5 - 0.0167 \cdot (\beta - 2)) \cdot \sin\left(\frac{\pi \cdot (\lambda + 0.1)}{18.5 - 0.3(\beta - 2)}\right) - 0.00184 \cdot (\lambda - 3) \cdot (\beta - 2) \quad (3)$$

$$\text{where: } \lambda = \frac{\Omega_t R}{V} \quad (4)$$

In the case of a variable speed, the variation of the power coefficient C_p as a function of λ for different values of the pitch angle β is illustrated in Fig.2.

The maximum value of $C_p(\lambda, \beta)$ is $C_{pmax} = 0.5$ for $\lambda_{opt} = 9.2$ and $\beta = 2$.

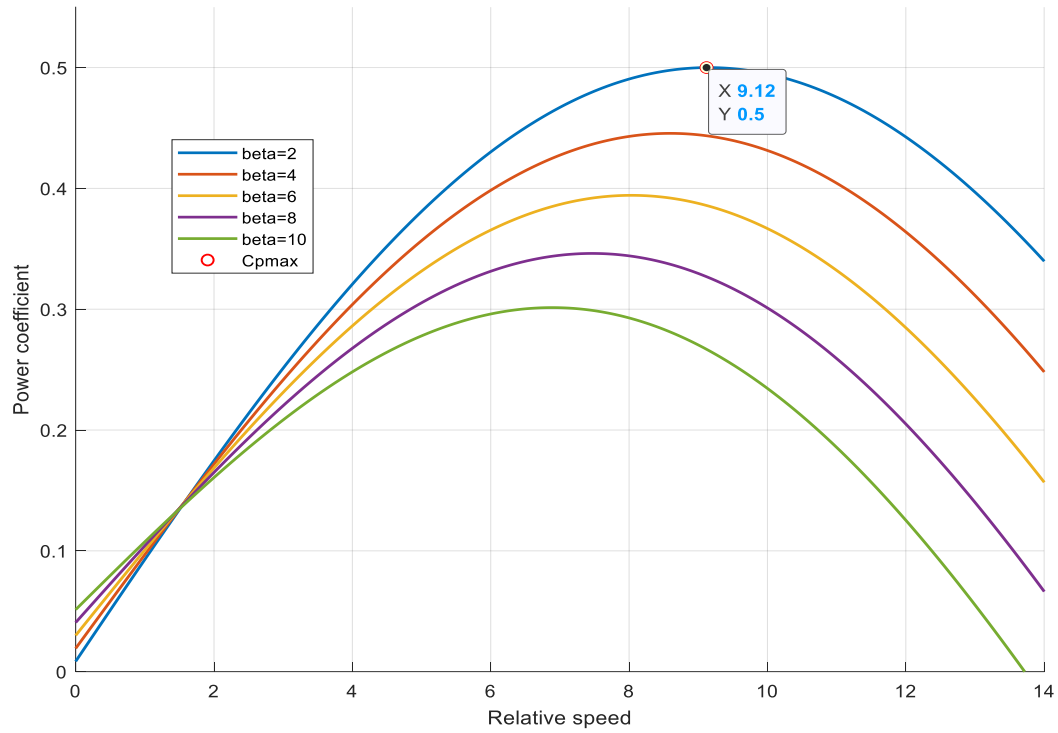


Fig. 2. Power Coefficient C_p .

The multiplier is represented by the gain (G), which adjusts the turbine's slow rotational speed to match the generator's higher mechanical speed. The overall inertia J is influenced by the generator's inertia J_g on the fast axis and the turbine's inertia J_t on the slow axis [1].

$$J = \frac{J_t}{G^2} + J_g \quad (5)$$

The electromagnetic and mechanical torques equation is given by:

$$J \frac{d\Omega_{mec}}{dt} = C_{mec} = C_g - C_{em} - C_f \quad (6)$$

where:

C_g : The torque from the multiplier is applied to the shaft of the generator

C_{em} : The electromagnetic torque produced by the generator

$C_f = f_v \Omega_{mec}$: The torque of viscous friction.

The turbine model is shown on the block diagram model below in Fig.3, regrouping the preceding equations [4,8,15,17].

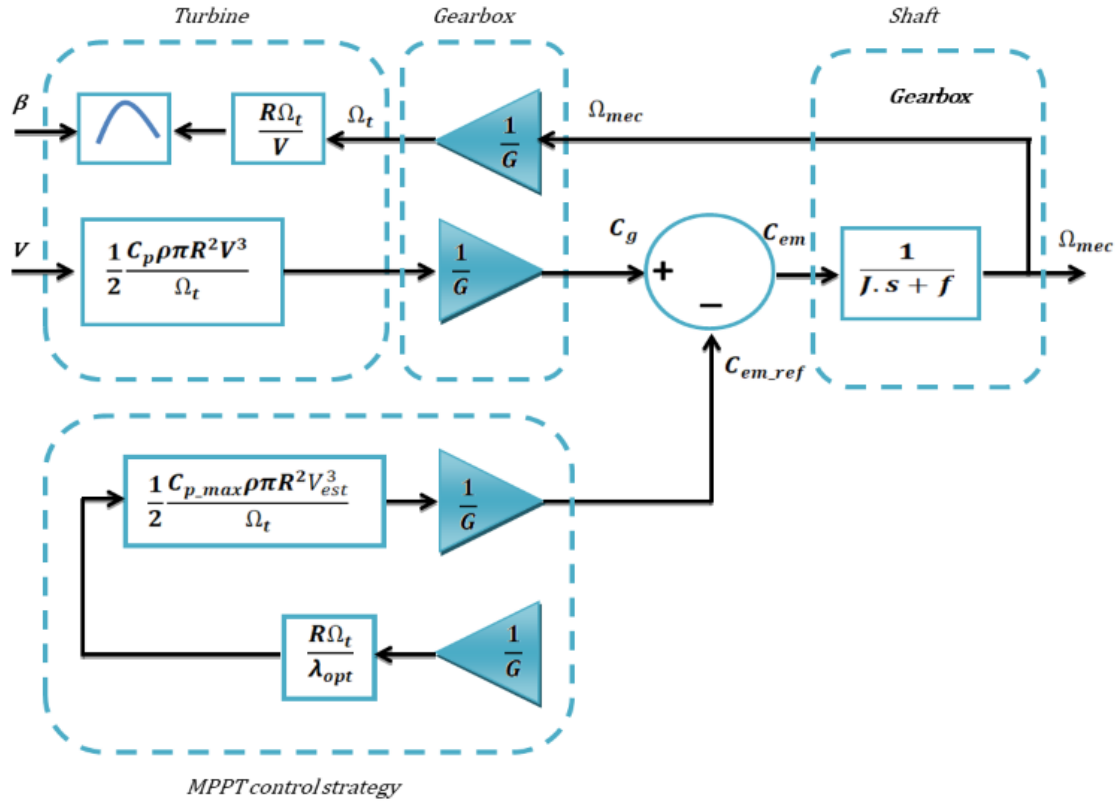


Fig.3. Schematic diagram of turbine-model with MPPT-control.

In order to optimize energy capture, it is crucial to constantly adapt the turbine's rotation speed to match the wind speed [11]. The idea behind this directive is to ensure the turbine is always rotating at an optimal speed ratio $\lambda = \lambda_{opt}$.

In this study, the turbine is regulated without speed control (Fig. 3). The electromagnetic torque reference C_{g_ref} is calculated based on an estimation of wind speed and the measurement of mechanical rotation speed [12].

$$\Omega_t = \frac{\Omega_{mec}}{G} \quad (7)$$

$$V = \frac{\Omega_{aer} R}{\lambda_{opt}} \quad (8)$$

$$C_{aer} = \frac{1}{2} C_c^{max} \rho \pi R^3 \quad (9)$$

$$C_{g_ref} = \frac{C_{aer_ref}}{G} = \frac{1}{2G\lambda_{opt}^2} C_c^{max} \rho \pi R^5 \Omega_t^2 \quad (10)$$

The DFIM mathematical model in d-q frame is presented as follows [15-17]:

$$\text{Stator voltages: } \begin{cases} V_{sd} = R_s \cdot i_{sd} + \frac{d\phi_{sd}}{dt} - \omega_s \cdot \phi_{sq} \\ V_{sq} = R_s \cdot i_{sq} + \frac{d\phi_{sq}}{dt} + \omega_s \cdot \phi_{sd} \end{cases} \quad (11)$$

$$\text{Rotor voltages: } \begin{cases} V_{rd} = R_r \cdot i_{rd} + \frac{d\phi_{rd}}{dt} - (\omega_s - \omega_r) \cdot \phi_{rq} \\ V_{rq} = R_r \cdot i_{rq} + \frac{d\phi_{rq}}{dt} + (\omega_s - \omega_r) \cdot \phi_{rd} \end{cases} \quad (12)$$

$$\text{Stator flux: } \begin{cases} \phi_{sd} = L_s \cdot i_{sd} + M \cdot i_{rd} \\ \phi_{sq} = L_s \cdot i_{sq} + M \cdot i_{rq} \end{cases} \quad (13)$$

$$\text{Rotor flux: } \begin{cases} \phi_{rd} = L_r \cdot i_{rd} + M \cdot i_{sd} \\ \phi_{rq} = L_r \cdot i_{rq} + M \cdot i_{sq} \end{cases} \quad (14)$$

$$\text{Stator powers: } \begin{cases} P_s = \frac{3}{2} (V_{sd} i_{sd} + V_{sq} i_{sq}) \\ Q_s = \frac{3}{2} (V_{sq} i_{sd} - V_{sd} i_{sq}) \end{cases} \quad (15)$$

where:

ω_s : The currents stator-pulsation, and ω_r : The currents rotor-pulsation.

The simplified model of the DFIG in Park reference (d-q) is shown in Fig.5 [3,8,9].

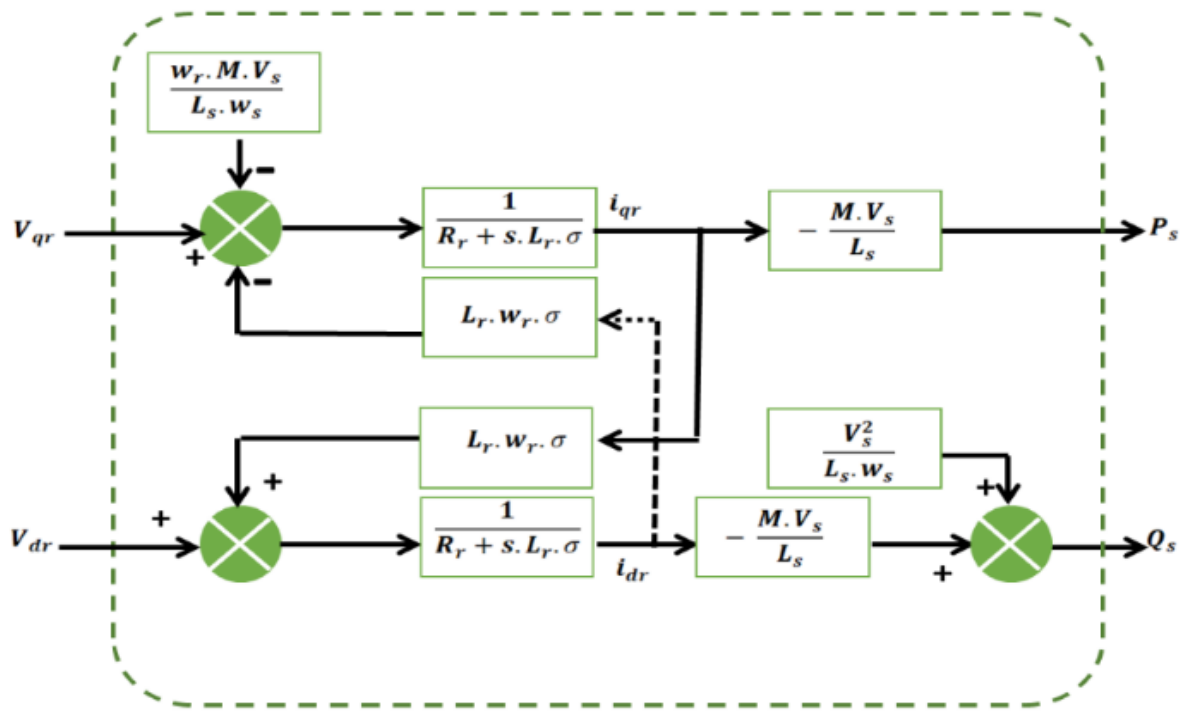


Fig. 5. Block diagram of DFIM in the Park-reference.

The PI-controller for DFIM combines proportional action to regulate system speed with integral action to close the gap between the desired setpoint and the actual output, enhancing control accuracy [6].

Two regulation loop functions are implemented for each axis, the first controlling the current and the second control the power (Fig.6) [6,10].

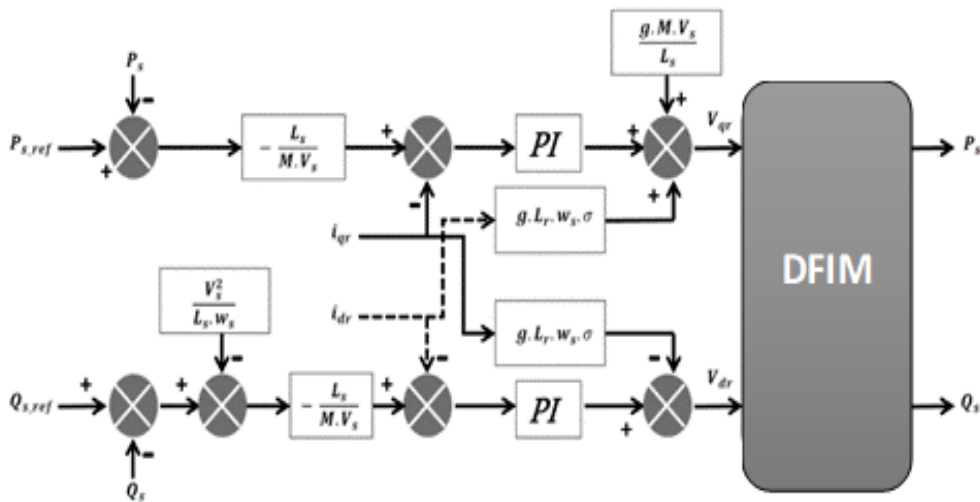


Fig. 6. Block diagram of Indirect Control with the Power Loop.

The Backstepping control design focuses on using "virtual control" to break down complex nonlinear control problems into simpler, more manageable components. It consists of sequential design steps, with each step referencing the previous one. Stability and performance are ensured through Lyapunov theory. To achieve precise control and effective power tracking despite parameter variations, integral action is incorporated, similar to methods for doubly fed induction generators. (Fig.7) [5,7,9].

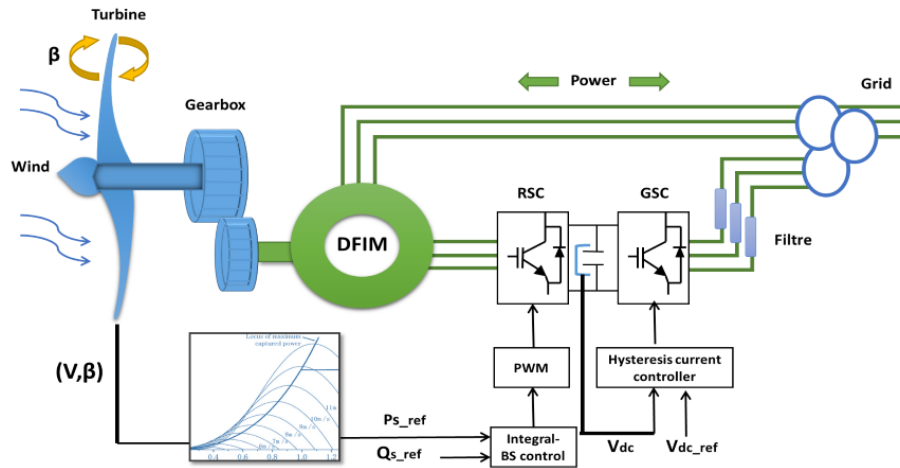


Fig. 7. Schematic diagram of Integral-BSC strategy for DFIM.

The Integral-Backstepping control is determined by the following expressions [14], where the error is defined as:

$$\begin{cases} e_p = P_s^* - P_s \\ e_q = Q_s^* - Q_s \end{cases} \quad (25)$$

Its derivative is:

$$\begin{cases} \dot{e}_{p0} = \dot{e}_p \\ \dot{e}_{q0} = \dot{e}_q \end{cases} \quad (26)$$

$$\begin{cases} e_{p0} = \lambda \int_0^t e_p(\tau) \cdot d\tau & \lambda > 0 \\ e_{q0} = \lambda \int_0^t e_q(\tau) \cdot d\tau & \lambda > 0 \end{cases} \quad (27)$$

The function of Lyapunov defines by:

$$\begin{cases} V(e_p) = \frac{1}{2} \cdot e_p^2 + \frac{1}{2} \cdot e_{p0}^2 \\ V(e_p, e_q) = \frac{1}{2} \cdot e_p^2 + \frac{1}{2} \cdot e_{p0}^2 + \frac{1}{2} \cdot e_q^2 + \frac{1}{2} \cdot e_{q0}^2 \end{cases} \quad (28)$$

Its derivative is:

$$\begin{cases} \dot{V}(e_p) = e_p(\dot{e}_p + \dot{e}_{p0}) \\ \dot{V}(e_p, e_q) = -k_p \cdot e_p^2 + e_q(\dot{e}_q + \dot{e}_{q0}) \end{cases} \quad (29)$$

With:

$$\begin{cases} \dot{e}_p = \dot{P}_s^* - \dot{P}_s = \dot{P}_s^* + \frac{\sigma \cdot L_s \cdot L_r}{M \cdot V_s} \cdot \frac{di_{rq}}{dt} \\ \dot{e}_q = \dot{Q}_s^* - \dot{Q}_s = \dot{Q}_s^* + \frac{\sigma \cdot L_s \cdot L_r}{M \cdot V_s} \cdot \frac{di_{rd}}{dt} \end{cases} \quad (30)$$

Replacing by its expression of the derivative of the current i_{rq} and i_{rd} , in the voltage V_{rq} and V_{rd} expressions, to obtain:

$$\begin{cases} \dot{e}_p = \dot{P}_s^* + \frac{M \cdot V_s}{\sigma \cdot L_s \cdot L_r} \cdot (V_{rq} - R_r \cdot i_{rq} - \sigma \cdot L_r \cdot \omega_r \cdot i_{rd} + g \cdot \frac{M \cdot V_s}{\omega_s \cdot L_s}) \\ \dot{e}_q = \dot{Q}_s^* + \frac{M \cdot V_s}{\sigma \cdot L_s \cdot L_r} \cdot (V_{rd} - R_r \cdot i_{rd} + \sigma \cdot L_r \cdot \omega_r \cdot i_{rq}) \end{cases} \quad (31)$$

Replacing the previous expression in (29):

$$\begin{cases} \dot{V}(e_p) = e_p \cdot \left(\dot{P}_s^* + \frac{M \cdot V_s}{\sigma \cdot L_s \cdot L_r} \cdot (V_{rq} - R_r \cdot i_{rq} - \sigma \cdot L_r \cdot \omega_r \cdot i_{rd} + g \cdot \frac{M \cdot V_s}{\omega_s \cdot L_s}) \right) + \dot{e}_{p0} \\ \dot{V}(e_p, e_q) = -k_p \cdot e_p^2 + e_q \cdot \left(\dot{Q}_s^* + \frac{M \cdot V_s}{\sigma \cdot L_s \cdot L_r} \cdot (V_{rd} - R_r \cdot i_{rd} + \sigma \cdot L_r \cdot \omega_r \cdot i_{rq}) \right) + \dot{e}_{q0} \end{cases} \quad (32)$$

The expressions of V_{rq} and V_{rd} are extracted as following:

$$\begin{cases} V_{rq} = -\frac{\sigma \cdot L_s \cdot L_r}{M \cdot V_s} \cdot \dot{P}_S^* + R_r \cdot i_{rq} + \sigma \cdot L_r \cdot \omega_r \cdot i_{rd} - g \cdot \frac{M \cdot V_s}{\omega_s \cdot L_s} - \frac{\sigma \cdot L_s \cdot L_r}{M \cdot V_s} \cdot (k_p \cdot e_p + e_{p0}) \\ V_{rd} = -\frac{\sigma \cdot L_s \cdot L_r}{M \cdot V_s} \cdot \dot{Q}_S^* + R_r \cdot i_{rd} - \sigma \cdot L_r \cdot \omega_r \cdot i_{rq} - \frac{\sigma \cdot L_s \cdot L_r}{M \cdot V_s} \cdot (k_q \cdot e_q + e_{q0}) \end{cases} \quad (33)$$

With:

$$\begin{cases} \dot{V}(e_p) = -k_p \cdot e_p^2 < 0 \\ \dot{V}(e_p, e_q) = -k_p \cdot e_p^2 - k_q \cdot e_q^2 < 0 \end{cases} \quad (34)$$

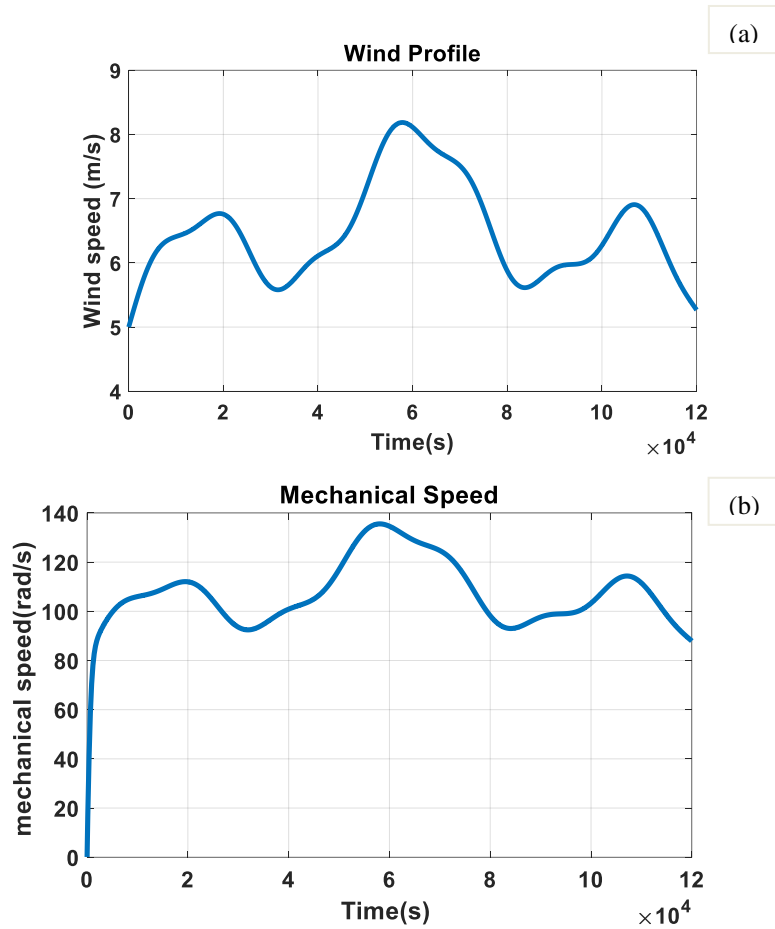
4. SIMULATION RESULTS

In this part, the wind-energy-conversion system (WECS) simulation is carried out using the MATLAB/Simulink platform. Both PI and integral-backstepping control techniques are utilized and evaluated for their ability to handle changes in DFIM parameters and track power references effectively.

A random wind profile is applied which varies between 5m/s and 9 m/s, as shown clearly in Fig.8. (a).

From Fig.8. (b), the mechanical speed extracting from the MPPT controller varies in the same shape as the wind speed.

The MPPT technique, kept the power coefficient C_p at its maximum value, which corresponds to $C_{pmax}=0.5$ for $\beta=2^\circ$ as shown in Fig.8.(c) and the relative speed still around $\lambda_{opt} = 9.2$ (Fig.8.(d)).



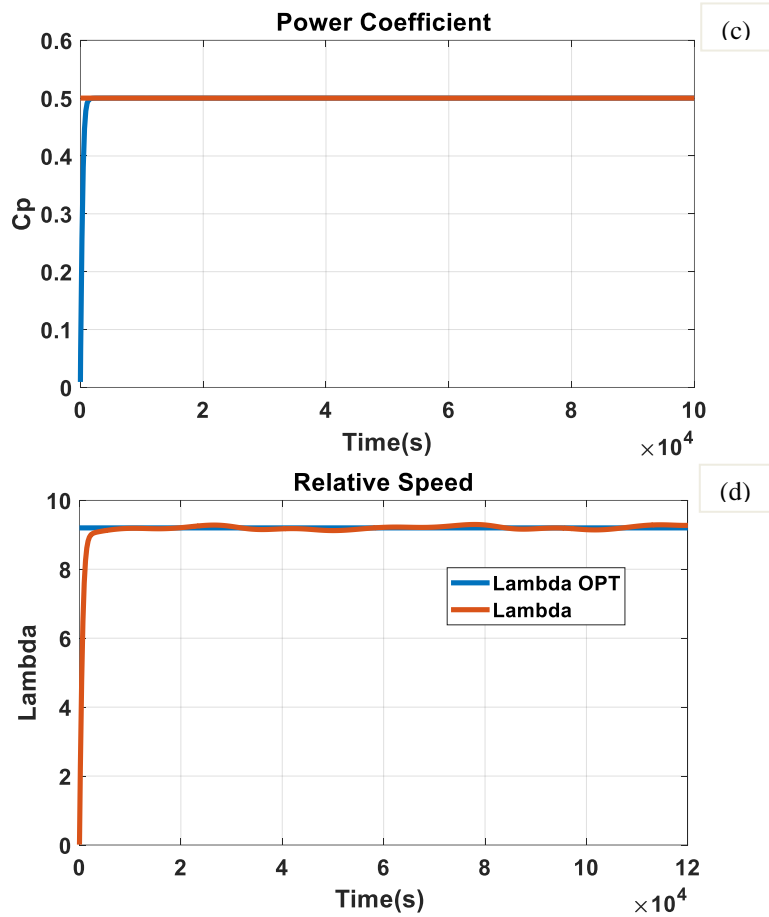
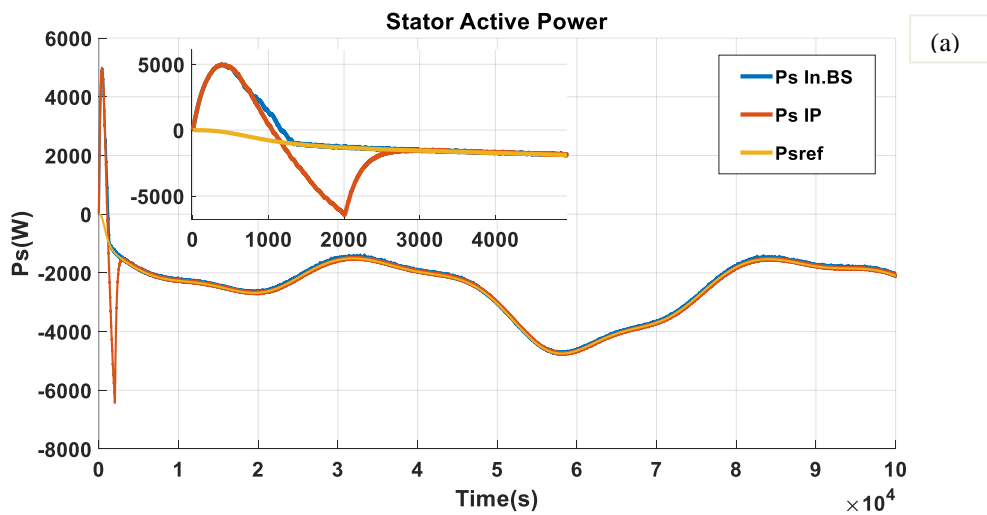


Fig. 8. Performance and System responses with MPPT strategy.

The results plotted show the powers generated with reference signals application.

Fig.9 shows the responses of the system for the indirect controller (PI) and the Integral Backstepping controller.



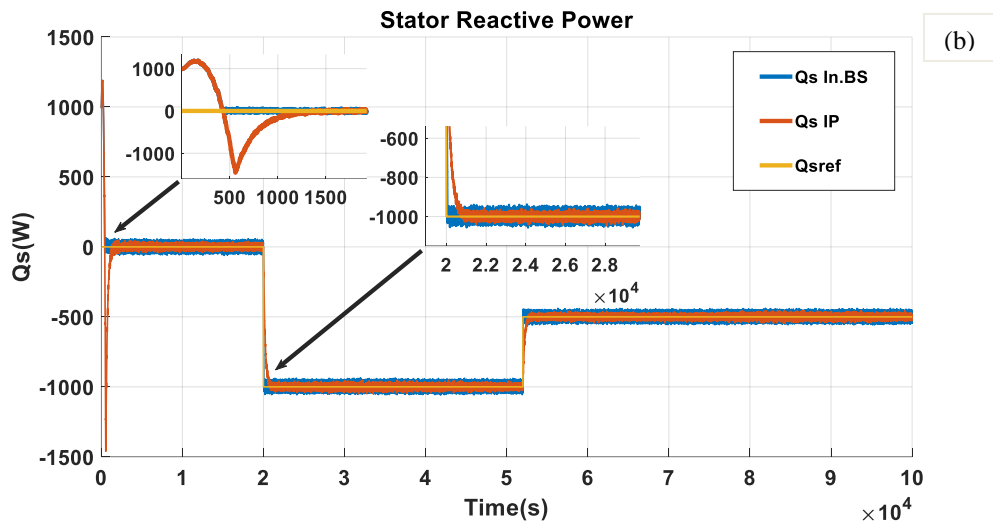


Fig. 9. System responses with Proportional-Integral (PI) and Integral Backstepping controller.

After analyzing the results, it is apparent that there is a complete separation between the active and reactive power.

The generator accurately monitors power instructions for both active and reactive powers.

In Fig.9. (a), shows the stator's active power tracking the wind profile and its reference set by the wind turbine, with a negative value indicating generator operation.

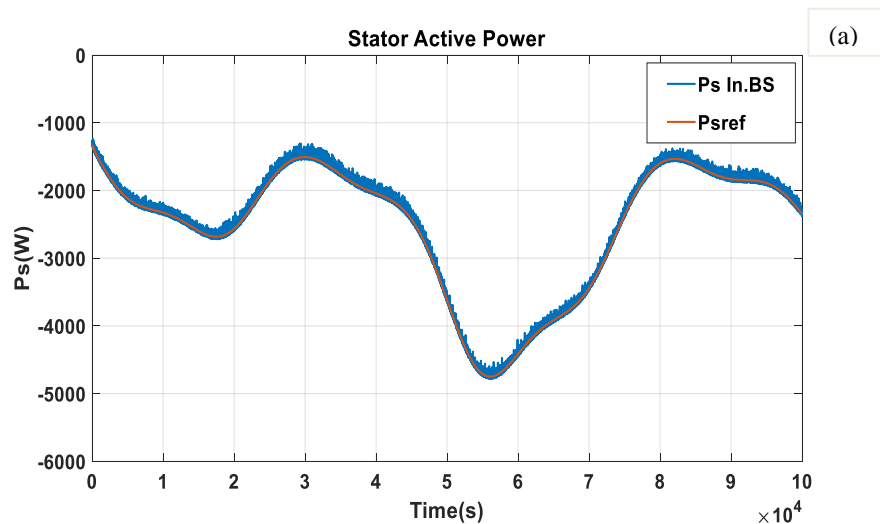
During the reference reactive power reference variation, the reactive power is modified in accordance with the network requirements as shown in Fig.9. (b).

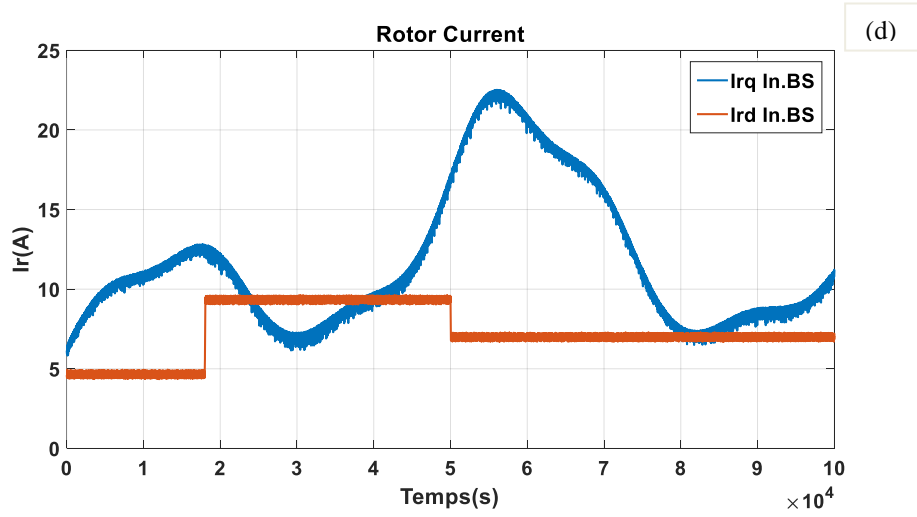
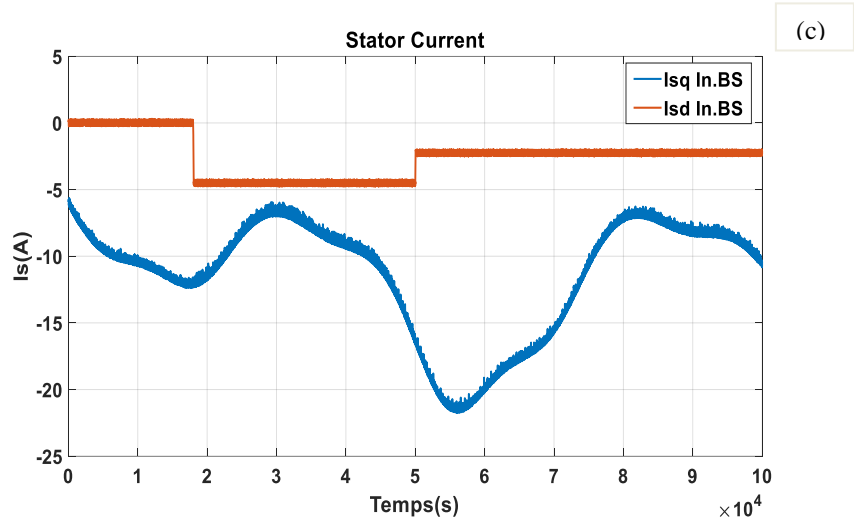
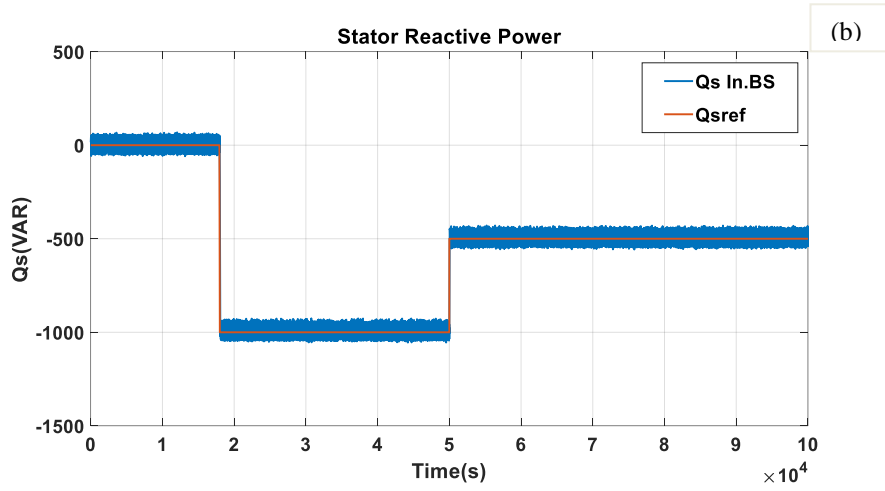
The simulation results show that the proposed Integral Backstepping control strategy surpasses the Proportional-Integral controller in variable wind conditions, exhibiting a more effective dynamic response. This improvement underscores the Integral Backstepping method's capability to adapt to fluctuating environmental factors, proving to be more effective than conventional control techniques in maintaining performance under changing conditions.

To evaluate the robustness of the Integral Backstepping control approach, testing was conducted under various conditions and scenarios., the values of stator and rotor resistances (R_s, R_r) and the mutual inductance M are doubled from its nominal values, (Fig.10) show the effect of parameter variations on the system performance.

These results show almost perfect track of reference and decoupling of the stator and rotor parameters: the active power in Fig.10. (a) and the reactive power in Fig.10. (b), the stator current and the rotor current from Fig.10. (c) and Fig.10. (d) respectively, and the power factor in the last figure (Fig.10.(e)), which confirming the robustness of Integral Backstepping controller the variations in these DFIG parameters do not significantly impact the power curves, and the power factor remains optimized throughout the testing process.

At the stator side, to ensure unity power factor and to optimize the quality of the energy produced on the grid, we maintained $Q_{s-ref} = 0$ VAR (Fig.11. (a)).





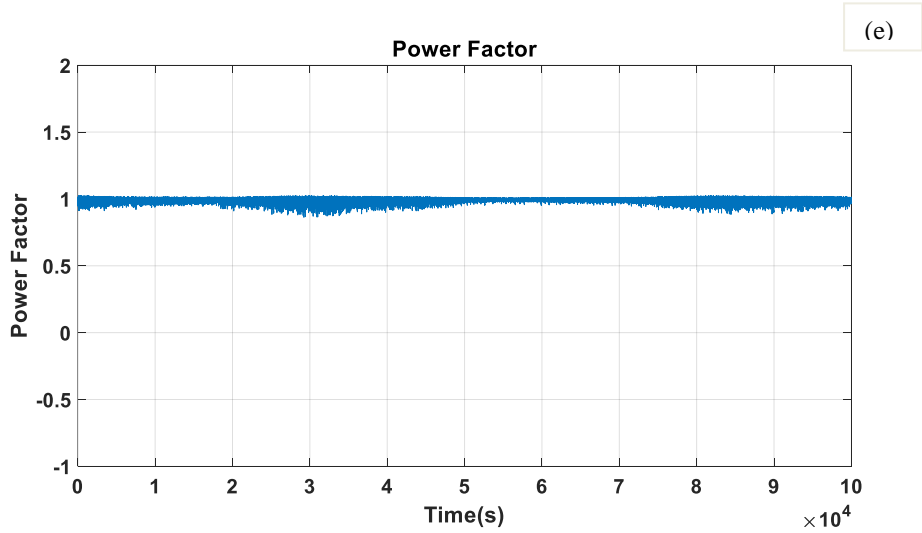
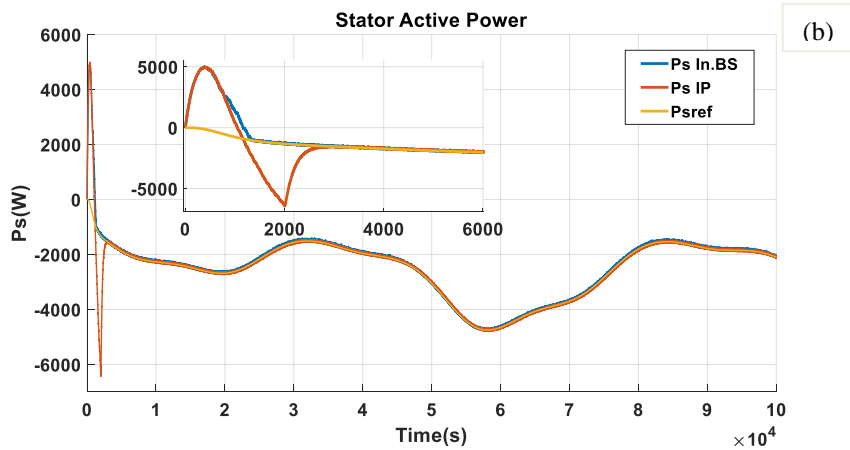
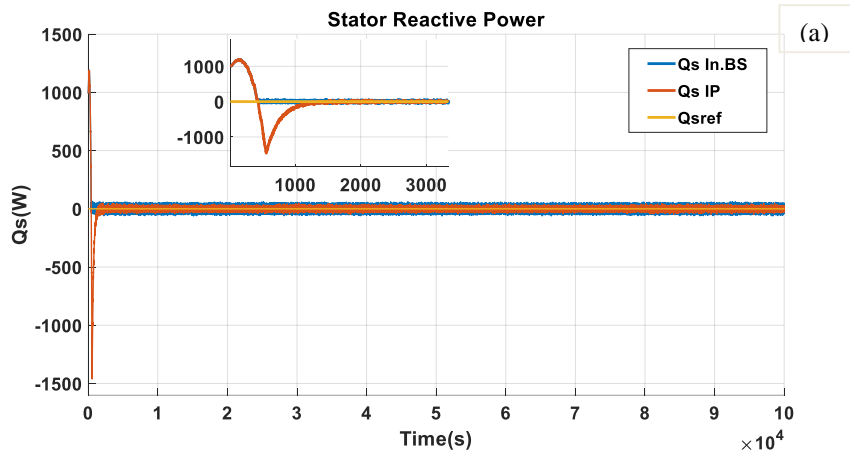


Fig.10. Test of robustness of stator resistance (+100% R_s), rotor resistance (+100% R_r) and mutual inductance variation (+100% M) using Integral Backstepping controller.



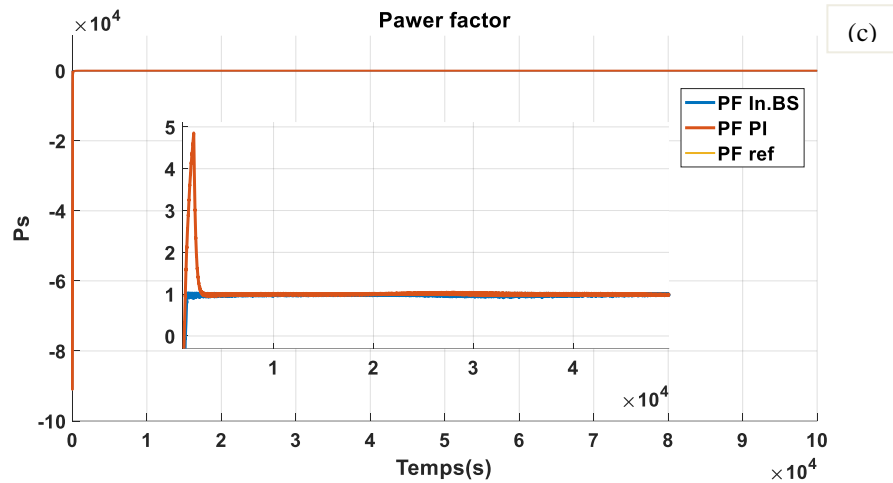


Fig.11. Power factor control.

Based on the simulation results, the stator reactive power in Fig.11.(a) and the stator active power in Fig.11.(b) are decoupled and track their references. However, some differences appear between the two control strategies, as the response times.

A unity power factor ($\cos(\phi)=1$) is perfectly achieved by the active power control for variable speed operation (Fig.11. (c)).

5. CONCLUSION

This paper examines both PI control and Integral Backstepping control strategies for managing the speed of variable-speed wind turbine systems. Using the Maximum Power Point Tracking (MPPT) technique, it effectively keeps the power coefficient (C_p) at its optimal level. Simulation results reveal that both control strategies enhance system performance, particularly in decoupling, reference tracking stability, and robustness against parameter fluctuations, while maintaining a unity power factor. Notably, the Integral Backstepping control outperforms the PI controller under variable wind conditions, demonstrating superior dynamic response, disturbance rejection, and resilience to parameter changes. This advantage ensures not only high performance but also more effective operation of the doubly fed induction generator. Overall, the findings underscore the Integral Backstepping control strategy as a more effective solution for speed control in wind turbine systems compared to traditional PI control, particularly in challenging and variable operational environments. The outcomes of the different simulations conducted were discussed and enabled the validation of the control mathematical representations of the suggested system.

REFERENCES

- [1] F. D. Bianchi, H. de Battista, R. J. Mantz, *Wind Turbine Control Systems: Principles, Modelling and Gain Scheduling Design*, 1st Edition, Advances in Industrial Control, Springer-Verlag, London Limited, 2007.
- [2] H. Jabbari Asl and J. Yoon, "Power capture optimization of variable-speed wind turbines using an output feedback controller," *Renewable Energy*, vol. 86, pp. 517-525, 2016.
- [3] M. Abolvafaei and S. Ganjefar, "Maximum power extraction from wind energy system using homotopy singular perturbation and fast terminal sliding mode method," *Renewable Energy*, vol. 148, pp. 611-626, 2020.
- [4] Y. Dvir and A. Levant, "Accelerated Twisting Algorithm," *IEEE Transactions on Automatic Control*, vol. 60, pp. 2803-2807, 2015.
- [5] J. Mérida, L. T. Aguilar and J. Dávila, "Analysis and synthesis of sliding mode control for large scale variable speed wind turbine for power optimization," *Renewable Energy*, vol. 71, pp. 715-728, 2014.
- [6] P. K. Ray, S. R. Paital, A. Mohanty, F. Y. Eddy, H. B. Gooi, "A robust power system stabilizer for enhancement of stability in power system using adaptive fuzzy sliding mode control," *Applied Soft Computing*, vol 73, pp. 471-81, 2018.
- [7] S. Bellarbi, D. S. Koussa and A. Djoudi, "Sliding Mode Control for PMSG-based Wind Power System," *Journal of Physics: Conference Series*, vol. 1081, p. 012012, 9 2018.
- [8] M. J. Morshed, and A. Fekih, "Design of a chattering-free integral terminal sliding mode approach for DFIG-based wind energy systems," *Optimal Control Applications and Methods*, vol 41(5), pp. 1718-34, 2020.
- [9] N. Cibiraj and M. Varatharajan, "Chattering reduction in sliding mode control of quadcopters using neural networks," *Energy Procedia*, vol. 117, pp. 885-892, 2017.

- [10] V. Utkin, A. Poznyak, Y. Orlov and A. Polyakov, "Conventional and high order sliding mode control," *Journal of the Franklin Institute*, vol. 357, pp. 10244-10261, 2020.
- [11] N.Zine Laabidine, B. Bossoufi, I. El Kafazi, C. El Bekkali, N. El Ouanjli, " Robust Adaptive Super Twisting Algorithm Sliding Mode Control of a Wind System Based on the PMSG Generator, " *Sustainability*, vol 15, 2023. <https://doi.org/10.3390/su151410792>
- [12] F. A. Patakor, M. Sulaiman and Z. Ibrahim, "Adaptive sliding mode for indirect field oriented controlled of induction motor," *Proceedings - 2011 IEEE Student Conference on Research and Development, SCORED 2011*, pp. 289-293, 2011.
- [13] S. Jeong and T. Hayashi, "Development of a wheeled inverted pendulum mobile platform with a four-bar parallel mechanism", *Adv. Robot.*, vol. 32, no. 4, pp. 191-201, Feb. 2018.
- [14] J. Rivera, L. Garcia, C. Mora, O. J. Raygoza and S. Ortega, *Super-Twisting Sliding Mode in Motion Control Systems*, A. Bartoszewicz, Ed., Rijeka, : IntechOpen, 2011.
- [15] S. Benelghali, M. E. H. Benbouzid, J. F. Charpentier, T. Ahmed-Ali and I. Munteanu, "Experimental Validation of a Marine Current Turbine Simulator: Application to a Permanent Magnet Synchronous Generator-Based System Second-Order Sliding Mode Control," *IEEE Transactions on Industrial Electronics*, vol. 58, pp. 118-126, 2011.
- [16] S. Kouadria, E. M. Berkouk, Y. Messlem and M. Denai, "Improved control strategy of DFIG-based wind turbines using direct torque and direct power control techniques," *Journal of Renewable and Sustainable Energy*, vol. 10, p. 043306, 2018.
- [17] B. Lahfaoui, S. Zouggar, B. Mohammed and M. L. Elhafyani, "Real Time Study of P&O MPPT Control for Small Wind PMSG Turbine Systems Using Arduino Microcontroller," *Energy Procedia*, vol. 111, pp. 1000-1009, 2017.
- [18] F. Mazouz, S. Belkacem, G. Boukhalfa, I. Colak, "Backstepping approach based on direct power control of a DFIG in WECS," In2021 10th International Conference on Renewable Energy Research and Application (ICRERA) 2021 Sep 26 (pp. 198-202). IEEE.
- [19] W. Sadara, B. Neammanee, "Control technique of back-to-back converter for DFIG in wind energy conversion system under abnormal voltage conditions, " *IEEJ Transactions on Electrical and Electronic Engineering*, vol 13(9), pp. 1285-95, 2018.
- [20] T. Sun, Z. Chen, F. Blaabjerg, "Transient stability of DFIG wind turbines at an external short-circuit fault, " *Wind energy*, vol 8(3), 345-60, 2005.
- [21] A. Maafa, H. Mellah, K. Benaouicha, B. Babes, A. Yahiou, H. Sahraoui, " Fuzzy Logic-Based Smart Control of Wind Energy Conversion System Using Cascaded Doubly Fed Induction Generator, " *Sustainability*, vol 16, 2024. <https://doi.org/10.3390/su16219333>
- [22] R. Rouabhi, A. Herizi, A. Djerioui, "Performance of Robust Type-2 Fuzzy Sliding Mode Control Compared to Various Conventional Controls of Doubly-Fed Induction Generator for Wind Power Conversion Systems, " *Energies*, vol 17, 2024. <https://doi.org/10.3390/en17153778>
- [23] H.M. Nguyen, "A Comparative Study of Different Sliding Mode Control Strategies for PMSG-Based Standalone WECS, " *International Journal of Renewable Energy Research (IJREER)*, vol 11(4), pp.1977-1986, 2021.
- [24] H. Moradi, Y. Alinejad-Beromi, H. Yaghoobi, and D. Bustan, "Sliding mode type-2 neuro-fuzzy power control of grid-connected DFIG for wind energy conversion system, " *IET Renewable Power Generation*, vol 13(13), pp.2435-2442, 2019.
- [25] Xu. Hu, S. Luo, Xi. Hu, and S. He, " Accelerated Adaptive Backstepping Control Based on the FWNN for the Multiple PMSGs System with Chaotic Oscillations, " *International Journal of Control, Automation and Systems*, vol 21(5), pp.1713-1725, 2023.